ISSN0511-5728
The West Indian Journal of Engineering
Vol.42, No.2, January 2020, pp.66-76

Investigating the Impact of Deformation on a 3D-printed Antenna in Biomedical Systems

Jeevan Persad[a] and Sean Rocke[b,Ψ]

Department of Electrical and Computer Engineering, The University of the West Indies, St. Augustine, Trinidad and Tobago, West Indies;

[a]Email: jeevan.persad.sta.uwi.edu
[b]Email: sean.rocke@sta.uwi.edu

[Ψ] *Corresponding Author*

(Received 29 April 2019; Revised 26 November 2019; Accepted 07 January 2020)

Abstract: *Recently, there has been increasing interest in using wearable sensors with flexible antennas. The antenna structures, which may be used for communications or for sensory elements, can possibly change their characteristics due to mechanical deformations. In this work, Radio frequency (RF) characteristics of a flexible Planar Inverted-F Antenna (PIFA) antenna intended for biomedical applications are explored. In the investigation, a traditional PIFA antenna structure on a Nylon substrate is considered. Using simulation studies, the flexible structure is subjected to various realistic mechanical deformations. Simulations facilitated investigation of the impact of the mechanical deformations on antenna performance, through consideration of the impact of flexibility on the reflection coefficient, transmission frequency and radiation patterns between 700MHz and 4GHz. Results demonstrated good stability on the antennas resonant frequency and physical resilience. However, increases in the reflection coefficient and the reach of the far-field as well as changes in the directionality of the antenna radiation pattern were observed as the antenna structure was pressed into the underlying tissue. These results provide valuable insights for those interested in deploying flexible antenna structures for wearable antenna and RF sensor applications.*

Keywords: *3D printing, antenna analysis, biosensor, body area networks, wearables*

1. Introduction

In recent years there has been an increased integration of technology into everyday aspects of our lives (Case, Burwick, Volpp, and Patel, 2015; Pantelopoulos and Bourbakis, 2010; Rais et al., 2009). As an example, this increased integration has resulted in devices becoming increasingly present in users' personal space, worn on the body of the user and integrated into the body of the user. As a consequence, there is a greater need to improve traditional electronics manufacturing to create devices that can adapt to a user's anatomy both internally and externally and also a need to examine the health effects of device usage. However, despite the challenges presented in the manufacturing of flexible electronic structures (Bandodkar, Jeerapan, and Wang, 2016) and ensuring their safe operation (Mertz, 2016), they present tremendous opportunities in the area of biomedical applications. In particular, monitoring human physiological function is becoming increasingly prevalent with devices emerging in the form of discrete sensors and complete systems (Pantelopoulos and Bourbakis, 2010).

Wearable devices in biomedical monitoring applications present significant opportunities for the continued monitoring of various physiological phenomena. Added benefit is gained when the information gathered through the devices can be analysed and visualised using remote applications (e.g., on the user's smart phone or on a medical practitioner's dashboard) (Pantelopoulos and Bourbakis, 2010; Salonen, Sydanheimo, Keskilammi, and Kivikoski, 1999). This exchange of information is facilitated through some form of communication system. For a great number of the remote applications the communication system is a form of wireless technology and a key component of the wireless communication system is the antenna. The design of the antenna for these wireless applications poses a significant challenge since there are concerns about antenna robustness, human safety and deterioration of the antenna performance as the wearer moves (Casula et al., 2017; Hall and Hao, 2006).

Considerable work has been undertaken to inform the construction and testing of antenna structures using flexible materials (e.g., Bai and Langley (2009, 2012), Bai, Rigelsford, and Langley (2013), Elias et al. (2013), and Sundarsingh et al. (2014)). The authors note that these studies have been limited in terms of the degree of distortion examined and the consideration given to the underlying tissue. Consequently, in this work, the impact of various induced deformations on the electromagnetic characteristics of antenna structures is examined. In

particular, the authors investigate the performance of a traditional Planar Inverted-F Antenna (PIFA) which has been adapted to a flexible substrate that can be produced using 3D printing manufacturing technologies.

It is noted that the analysis can be extended to other antenna structures. Investigations are performed via simulation studies using COMSOL Multiphysics software. The substrate material chosen was Nylon which is a readily available 3D printing material and has been frequently adapted to antenna structures (Hertleer et al., 2007; Matthews and Pettitt, 2009; Shakhirul et al., 2014). Deformation of the structure is examined for forces pressed into the skin surface and for forces acting up out of the skin surface due to for example, a bending joint. The investigations provide valuable insights for factoring into the design and use of wearable Very Low Frequency (VLF) to Ultra High Frequency (UHF) devices.

The paper is structured as follows. A brief literature review is presented along with the motivation behind the work. This is followed by the methodology and a description of the modelling work. Finally, the simulated results are presented and discussed.

2. Related Work

The examination of the antenna performance under instances of deformation is important when one considers that the modification of the antenna structure caused by the deformation can result in changes in antenna performance including shifting of resonant frequencies, varying radiation patterns and varying S-parameters (Rais et al., 2009). When these variations in antenna characteristics occur the ability of the antenna to function is compromised which can lead to significant performance degradation and/or unsafe operational conditions (Rogier, 2015; Soh et al., 2012).

Several studies have been undertaken which focus specifically on the deformation of wearable antennas. In much of the existing body of work, researchers have examined simple deformation patterns of the antenna structure with an emphasis on deformations in a single plane. In Bai and Langley (2009), the behaviour of a dual band Coplanar Waveguide Fed (CPW) antenna was examined under bending and crumpling conditions where deformations were examined on a single plane and no body model was considered. In Bai and Langley (2012), the performance of a PIFA antenna, centre frequency 2.4GHz, was observed under crumpling conditions and a simple human body model (HBM) was used to examine human interaction.

However, the crumpling pattern was examined on a single plane and the antenna structure was modelled as being 5 mm above the HBM. The electromagnetic structure considered in Bai et al. (2013) was a microstrip patch array which was subjected to crumpling and a phantom was used for human body simulations. As with the previous studies, the crumpling pattern was examined on a single plane and the antenna structure was not placed against the model surface but was suspended 3mm above. Elias et al. (2013) examined the crumpling of a dipole antenna, centre frequency 2.4GHz, a body model was used to consider the impact of human tissue. The crumpling pattern was examined on a single plane and the antenna was not placed on the surface of the body model but was suspended 1 mm above. Finally, in Sundarsingh et al. (2014), a GSM-900 and 1800 dual-band patch antenna was studied under bending and crumpling conditions and a rectangular 3 layer body model was used for the human study. The bends and crumpling were examined on a single plane and the deformed antenna structure was not considered with the body model.

Additionally, in the literature, there has not been considerable investigation of the surrounding antenna environment. For the specific case of human tissue interaction, researchers utilised simulation models and phantoms but no study considered the effect of the antenna directly on the body. Finally, to the authors' knowledge, no body of work has examined the behaviour of such antenna structures while considering complex multi-planar deformations due to the body tissue and muscle movement where the underlying body tissue is also deformed.

To address these gaps, in this study a PIFA antenna structure was considered as being worn on the user's skin. The deformation of the antenna structure was investigated for forces pressed into the skin surface and for forces acting up out of the skin surface due to for example a bending joint. The impact of these deformations on antenna characteristics was then investigated.

3. Methodology

For the study an existing Planar Inverted-F Antenna (PIFA) design as proposed in Bai and Langley (2012) with a resonant frequency of 2.4GHz was considered under two distinct deformation conditions across the frequency range of 700MHz–4GHz. The deformation conditions were application of external forces acting on the wearer's skin (i.e., pressing forces) and forces from within the wearer's body (e.g., bicep bulging, skin folding and elbow joint bending body forces). The study was conducted using simulation tools due to the complexity of the antenna geometry and the expected irregularity of the distorted antenna structure. In this study the antenna is considered to be directly secured to the tissue surface (epidermis). For the purpose of the study the reflection coefficient, transmission frequency and radiation pattern of the PIFA were examined before and after distortion due to the application of pressing and body forces. The general antenna features, simulation modelling assumptions and model setup are described in the following sections.

3.1. Theory of Operation

The Planar Inverted-F Antenna (PIFA) is one of the most popular antenna structures used in mobile devices Bevelacqua (2016). The PIFA achieves resonance at roughly a quarter wavelength, which allows it to have a significantly smaller footprint. The specific Planar Inverted-F Antenna (PIFA) used in this study was adapted from the work described in Bai and Langley (2012). The previous PIFA design was intended for a textile adaptation with centre frequency of 2.4GHz which is suitable for wireless applications. Therefore, the design was selected due to its desirable resonant frequency and previous evaluation on a flexible substrate intended for a body worn applications. Since the goal of the extended work is to ultimately manufacture the antenna and support electronics using 3D printing techniques, the substrate was chosen to be Nylon. Nylon as a material is compatible with many 3D printing processes and is readily available from multiple suppliers. The material has also been frequently adapted as a substrate for antenna structures (Andreuccetti, Fossi, and Petrucci, 1997; Hertleer et al., 2007; Liang and Boppart, 2010; Matthews and Pettitt, 2009; Shakhirul et al., 2014).

Figure 1 shows the basic PIFA antenna structure. The impedance of the antenna is controlled by D3, the distance between the short pin and the feed point.

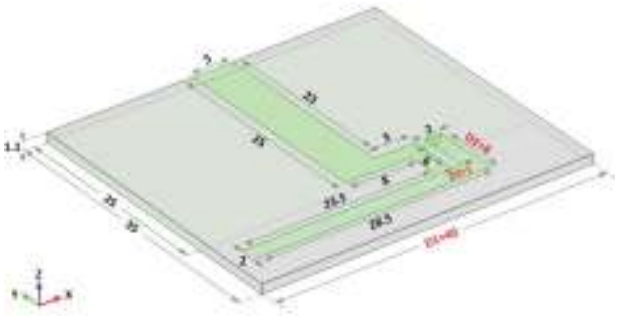

Figure 1. PIFA antenna structure

If one were to consider the radiation pattern of the antenna structure to be along its edge then the resonant length of the PIFA would be given by Bevelacqua (2016):

$$D1 + D2 = \frac{\lambda}{4} \tag{1}$$

where λ is the wavelength of the resonant frequency *f*. The resonant frequency would be given by:

$$f = \frac{c}{(4\sqrt{\epsilon_r}(D1+D2))} \tag{2}$$

where c is the speed of light in a vacuum and ϵ_r is the relative permittivity of the antenna substrate.

Antenna performance can be affected by changes in geometry due to deformations (e.g., substrate stretching and folding) which can affect distances such as the distance between the feed point and short pin, (i.e., *D3*) as well as changes in material properties such as effective permittivity due to the operating environment (e.g., moisture/humidity) and effects of human tissue Rogier (2015). In this work the emphasis is on the impact of deformations and as such the effects of other factors are not studied.

3.2. Model details

An antenna structure serves to couple currents to electromagnetic waves to facilitate either radiation or reception. The behaviour of the associated electric and magnetic waves is governed by complicated solutions of Maxwell's equations for applied boundary conditions Balanis (1992):

$$\bar{E}.\bar{dl} = -\frac{d}{dt}\int_S B.dS \tag{3}$$

$$\bar{H}.\bar{dl} = \int_S J.dS + \frac{d}{dt}\int_S D.dS \tag{4}$$

While paper-based analysis using antenna theory is possible this approach is not suitable to the analysis of the current distribution in an irregularly distorted antenna structure. Thus, due to the complexity of the antenna distortions a 3D simulation model of the antenna was created.

Similarly, for the mechanical deformation of the human tissue there are several factors which would impact the behaviour of the tissue layers. For example, in the work undertaken by Liang and Boppart (2010) an expression was proposed for displacement in a single plane (z-axis) based on the harmonic excitation of skin tissue as an infinite elastic homogenous layer:

$$u_z = R_e\left\{\frac{\partial\phi}{\partial z} + \frac{\partial H_z}{\partial x}\right\} = (Ae^{-qz} - 2sqe^{-sz})\cos(k_R x - \omega t) \tag{5}$$

where ϕ and H_z are potentials, k_R is the wavenumber of the surface wave propagating on the skin, ω is the driving angular frequency and A, s and q are parameters to be computed. Due to the computational complexity of calculating the deformations across more than one plane, simulation tools were utilised. The simulation software utilized was the COMSOL Multiphysics tool. The COMSOL software allows crosscutting studies integrating different disciplines, in this case, Mechanical and Electrical facilitating the simultaneous examination of the physical and electromagnetic behaviour of models. The simulation model used for the study is shown in Figure 2.

The dimensional and material details which were used in building the model are captured in Table 1 Andreuccetti et al. (1997), where *P* is material density, *E* is Young's modulus, v is Poissons ratio, ϵ_r is material permittivity, σ is material conductivity. For the purposes of this study the frequency range of 700MHz - 4GHz was used. The body model as presented in the simulation

represents a blood vessel which is located close to the skin surface on the forearm.

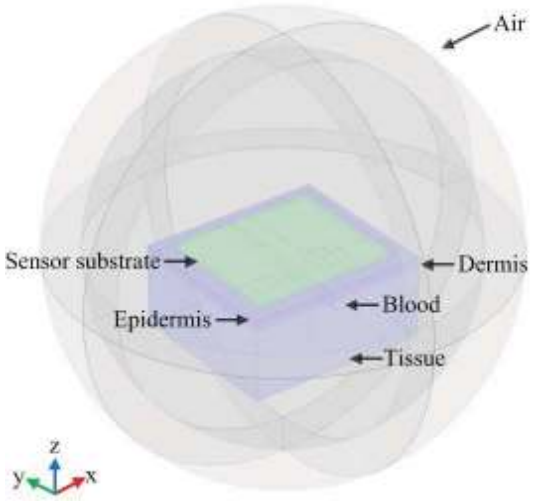

Figure 2. PIFA Antenna and body model used for the study

Table 1. Dimensional and material details used in the model

Dimensions (L,W,H)	Mechanical Parameters	Electrical Parameters
Air		
dia. 60.0mm, 50.0mm		
Substrate (Nylon)		
40.0mm 35.0mm 1.1mm	P = 1150[kg/m^3] E = 2e9[Pa] v = 0.4	σ = 1.0e - 11[S/m] ϵ_r = 4.0
Epidermis		
50.0mm 45.0mm 1.1mm	P = 1190[kg/m^3] E = 102e6[Pa] v = 0.47	σ = 1.8e - 2[S/m] ϵ_r = 31
Dermis		
50.0mm 45.0mm 1.5mm	P = 1116[kg/m^3] E = 102e5[Pa] v = 0.47	σ = 4.3e - 1[S/m] ϵ_r = 40
Tissue		
50.0mm 45.0mm 20.0mm	P = 971[kg/m^3] E = 102e2[Pa] v = 0.48	σ = 1.5e - 1[S/m] ϵ_r = 17
Blood Vessel		
dia. 3.2mm, 45mm	P = 1060[kg/m^3] E = 6e4[Pa] v = 0.4	σ = 4.3e - 1[S/m] ϵ_r = 65

3.3. Test Cases

The antenna and body model was considered under conditions of external forces acting on the antenna (pressing forces) and forces from within the wearers body (body forces). For both distortion scenarios the surface of the antenna face was divided into nine overlapping regions as shown in Figure 3. The pressing and body forces were then applied to each region.

In considering the pressing force the specific scenario of an index finger pressing downward was examined. The pressing force created would vary based on an individual's age, sex and other demographics Peebles and Norris (2003) and for this work a uniform loading of 40N was used. The average finger dimension of 25 mm as found in Murai et al. (1997) was used. In considering the body acting forces the specific scenario of a bicep muscle contracting was considered. The contraction is a function of the movement of the forearm in which the bulging of the bicep muscle transmits a force through the layers of tissue. The force produced varies based on several factors including the degree of exertion and various individual demographic factors such as age, sex, level of fitness (Cameron et al., 1993) and for this work a uniform loading of 30N was used (Shima et al., 2009). The zoning of the body acting forces was developed based on the antenna being placed in varying positions above the bicep region.

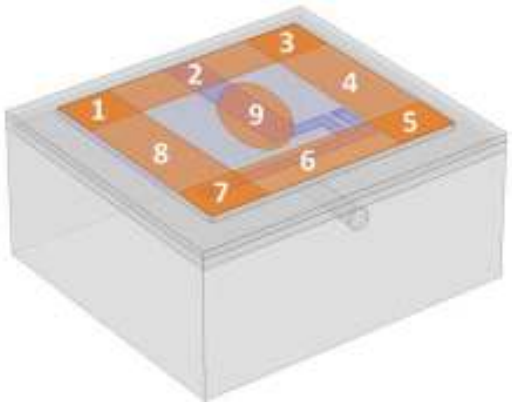

Figure 3. Nine (9) regions of force application onto the antenna face

For each simulation scenario the radiation pattern in the x-y, x-z, y-z planes, resonant frequency f_r and reflection coefficient S_{11} of the undistorted and distorted model were calculated and compared for the frequency range of 700MHz-4GHz in 50MHz steps.

4. Results

Figures 4 and 5 show examples of the 3D displacement plots generated in COMSOL for forces applied to the regions identified in Figure 3, due to the action of the body forces and press forces, respectively. The plots also record the maximum displacement (mm) for each of the distortion scenarios. The figures also illustrate the radiation plots in the x-y, x-z and y-z planes for three selected frequencies: 1GHz, 3GHz, 4GHz before and after the application of the respective forces.

For the displacement plots of the pressing forces, it was observed that the antenna structure was pressed into the underlying epidermis and dermis at each of the affected regions. For the pressing forces the average maximum displacement was approximately 2.74 mm with the greatest displacement of 3.16 mm being observed at regions 4 and 8. A significantly smaller

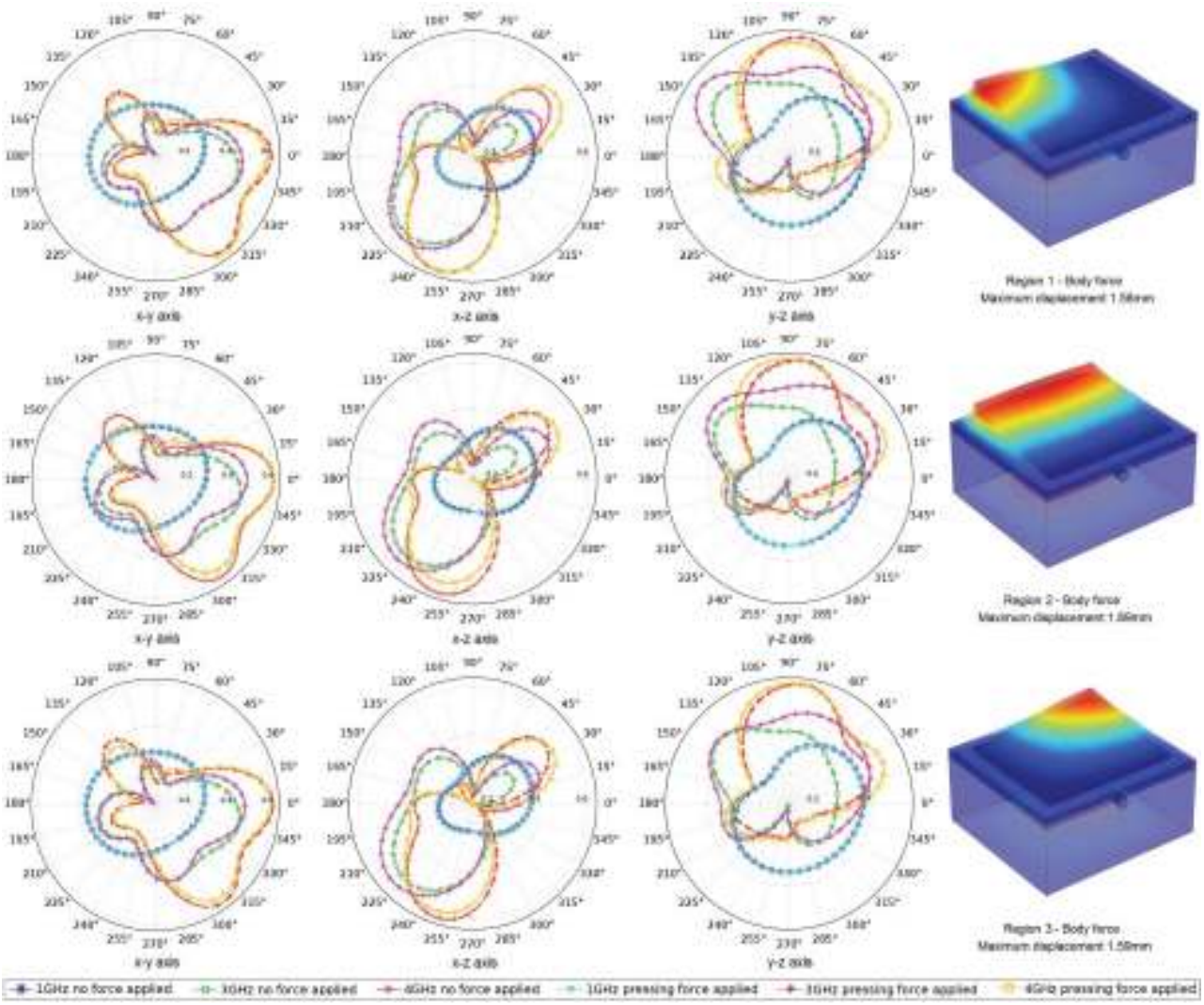

Figure 4. Plots of the antenna radiation pattern in the x-y, x-z, y-z planes and maximum displacement for the action of body forces, applied to Regions 1-3

displacement of 0.20mm was observed for region 9 of the antenna surface. For the displacement plots of the body forces, it was observed that the antenna structure was bent outward at the point of action of the force. For the body forces the average maximum displacement was approximately 1.77mm with the greatest displacement of 2.00mm being observed at regions 4 and 8. The minimum displacement observed was 0.57 mm at region 9.

Significant change in the radiation pattern for the three planes was observed at the higher frequencies of 3GHz and 4GHz due to the application of the pressing force. For the radiation plots at 1GHz involving the application of the pressing force, it was observed that the radiation pattern in all three planes was relatively symmetric. Furthermore, no significant deviation in the radiation pattern was observed due to the bending of the antenna and distortion of the underlying tissue caused by the application of the pressing force. In contrast, for the radiation plots at 3GHz and 4GHz respectively, it was observed that the patterns grew increasingly distorted and extended further afield as the frequency increased.

For the radiation plots at 1GHz involving the application of the body force, the radiation pattern in all three planes was observed to be relatively symmetric. Furthermore, at 1GHz, no significant deviation in the radiation pattern was observed due to the action of the body force on the antenna and the underlying tissue. For the higher frequency plots at 3GHz and 4GHz respectively, the radiation pattern was observed to be significantly less symmetric as compared to the lower frequency and extended further afield. Furthermore, it was observed that the radiation pattern plots at 3GHz and 4GHz showed significant variation as a result of the tissue motion and antenna bending caused by the applied body force.

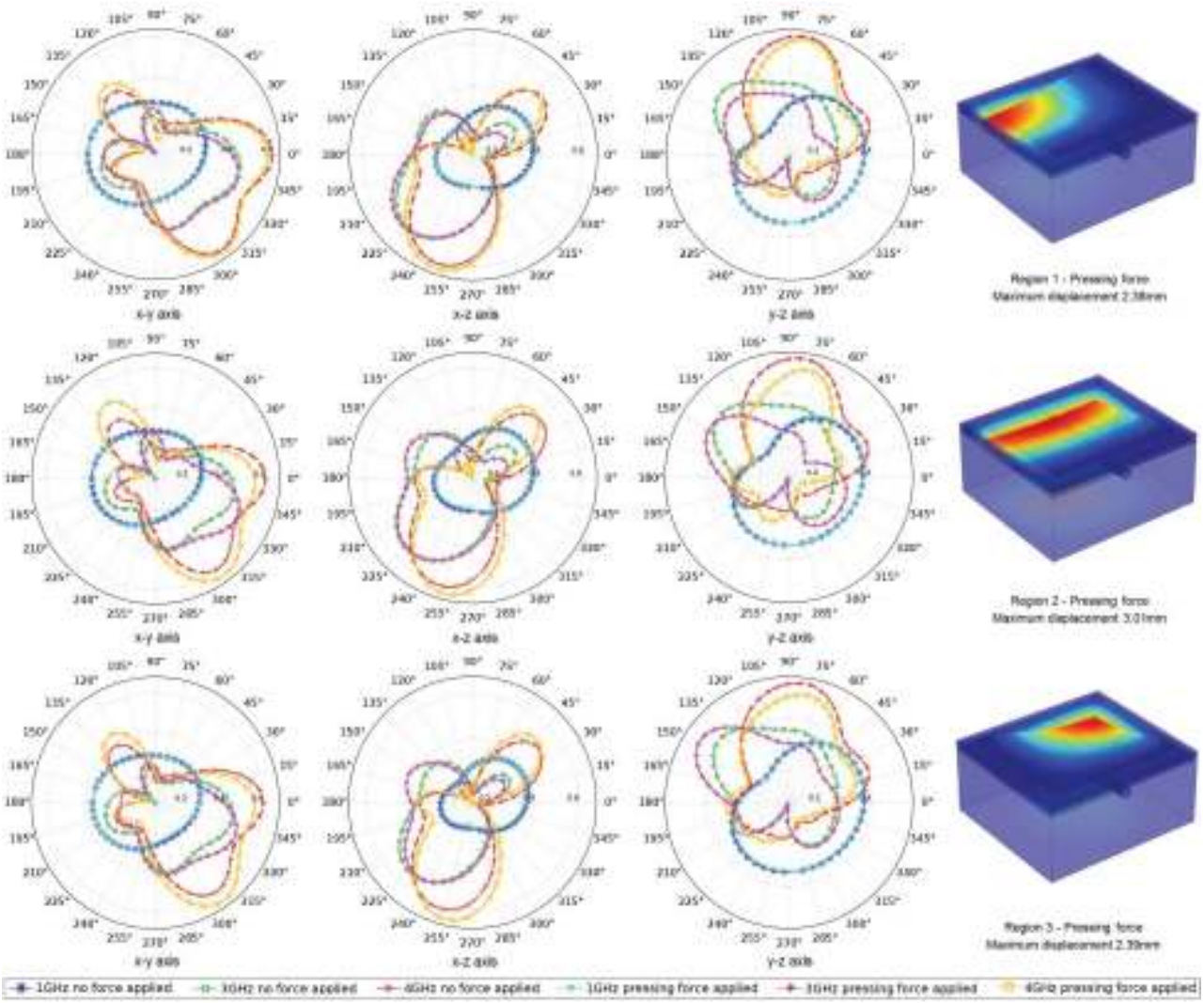

Figure 5. Plots of the antenna radiation pattern in the x-y, x-z, y-z planes and maximum displacement for the action of pressing forces, applied to Regions 1-3

Tables 2-4 summarise the Mean Square Error (MSE) calculations for the normalized far-field radiations plots for the press force (x-y, x-z, y-z planes) and the body force (x-y, x-z, y-z planes) as well as for the 3-dimension volume. The MSE was chosen to give a quantitative measure of the degree to which the radiation patterns deviate from the undisturbed antenna structure (i.e. with no applied forces) as a result of deformations induced by the applied forces. The calculated MSE values (for both the planes as well as the 3D volume) showed an increase as the signal frequency was increased. The increase in the MSE values was noted for application of the press force as well as for the body force.

Table 2. MSE values for the normalised far-field in the x-y, x-z, y-z planes for the press force. D_{press} denotes the displacement in mm

Region	D_{press}	MSE Far-field norm 1GHz, x-y plane	MSE Far-field norm 3GHz, x-y plane	MSE Far-field norm 4GHz, x-y plane	MSE Far-field norm 1GHz, x-z plane	MSE Far-field norm 3GHz, x-z plane	MSE Far-field norm 4GHz, x-z plane	MSE Far-field norm 1GHz, y-z plane	MSE Far-field norm 3GHz, y-z plane	MSE Far-field norm 4GHz, y-z plane
1	2.38	3.61E-05	1.19E-03	6.76E-04	2.79E-05	6.88E-04	9.74E-04	3.49E-05	1.33E-03	1.07E-03
2	3.01	3.54E-05	2.71E-03	1.90E-03	3.14E-05	1.59E-03	2.85E-03	4.85E-05	2.39E-03	2.44E-03
3	2.39	6.35E-06	6.07E-04	8.94E-04	3.74E-05	7.92E-04	1.31E-03	9.79E-06	5.46E-04	9.12E-04
4	3.16	2.19E-05	6.94E-04	2.81E-03	5.12E-05	8.63E-04	4.80E-03	8.82E-06	6.22E-04	3.04E-03
5	2.39	1.34E-05	2.73E-04	5.13E-04	9.43E-06	6.14E-04	1.40E-03	6.32E-06	5.29E-04	7.91E-04
6	3.01	2.80E-04	6.60E-03	5.82E-03	3.82E-05	3.98E-03	4.10E-03	3.66E-05	7.29E-03	3.48E-03
7	2.40	1.85E-04	2.98E-03	3.20E-03	1.02E-05	1.69E-03	2.75E-03	1.55E-05	2.87E-03	2.05E-03
8	3.16	3.48E-04	6.94E-03	9.73E-03	6.60E-05	3.79E-03	5.28E-03	1.06E-04	5.41E-03	6.72E-03
9	0.20	8.01E-07	5.73E-06	1.48E-05	1.16E-06	1.12E-05	1.87E-05	1.14E-06	1.21E-05	1.19E-05

Table 3. MSE values for the normalised far-field in the x-y, x-z, y-z planes for the body force. D_{body} denotes the displacement in mm

Region	D_{body}	MSE Far-field norm 1GHz, x-y plane	MSE Far-field norm 3GHz, x-y plane	MSE Far-field norm 4GHz, x-y plane	MSE Far-field norm 1GHz, x-z plane	MSE Far-field norm 3GHz, x-z plane	MSE Far-field norm 4GHz, x-z plane	MSE Far-field norm 1GHz, y-z plane	MSE Far-field norm 3GHz, y-z plane	MSE Far-field norm 4GHz, y-z plane
1	1.58	9.79E-06	1.86E-03	4.38E-04	1.75E-05	3.29E-03	8.62E-04	1.44E-05	2.91E-03	7.08E-04
2	1.89	8.69E-06	2.55E-03	8.32E-04	1.32E-05	5.64E-03	1.51E-03	1.54E-05	4.21E-03	1.23E-03
3	1.59	2.85E-06	1.22E-03	2.36E-04	1.03E-05	3.50E-03	8.13E-04	4.80E-06	1.98E-03	4.75E-04
4	2.00	1.44E-05	1.01E-03	7.56E-04	1.65E-05	2.08E-03	2.06E-03	1.31E-05	1.31E-03	8.37E-04
5	1.59	1.70E-05	6.48E-04	4.51E-04	4.09E-06	1.47E-03	1.07E-03	1.73E-05	9.25E-04	4.68E-04
6	1.89	3.91E-04	3.96E-03	7.98E-03	8.27E-05	1.72E-03	3.16E-03	5.87E-05	2.00E-03	2.59E-03
7	1.59	6.23E-05	1.60E-03	1.78E-03	4.97E-06	1.16E-03	1.74E-03	2.37E-05	1.40E-03	1.23E-03
8	2.00	1.11E-04	4.80E-03	3.22E-03	3.03E-05	2.51E-03	2.99E-03	6.15E-05	4.22E-03	2.32E-03
9	0.57	4.52E-06	7.31E-04	2.06E-04	3.16E-06	1.98E-03	5.42E-04	7.66E-06	1.21E-03	3.05E-04

Table 4. MSE values for the normalised far-field of the 3d volume

			Press force			Body force		
Region	D_{press}	D_{body}	MSE Far-field norm 1GHz	MSE Far-field norm 3GHz	MSE Far-field norm 4GHz	MSE Far-field norm 1GHz	MSE Far-field norm 3GHz	MSE Far-field norm 4GHz
1	2.38	1.58	4.30E-05	9.87E-04	9.51E-04	1.34E-05	1.76E-03	4.55E-04
2	3.01	1.89	5.60E-05	1.95E-03	2.41E-03	1.38E-05	2.53E-03	1.14E-03
3	2.39	1.59	9.95E-06	5.12E-04	1.11E-03	3.44E-06	1.11E-03	4.54E-04
4	3.16	2.00	1.65E-05	7.58E-04	3.26E-03	1.42E-05	7.63E-04	1.08E-03
5	2.39	1.59	8.24E-06	5.06E-04	7.91E-04	1.77E-05	5.15E-04	4.83E-04
6	3.01	1.89	5.96E-05	7.89E-03	4.17E-03	2.43E-04	3.26E-03	4.59E-03
7	2.40	1.59	4.00E-05	3.36E-03	2.30E-03	4.18E-05	1.34E-03	1.26E-03
8	3.16	2.00	1.51E-04	6.38E-03	6.96E-03	8.36E-05	4.05E-03	2.23E-03
9	0.20	0.57	1.19E-06	9.40E-06	1.40E-05	6.54E-06	6.46E-04	2.10E-04

For the 1GHz signal frequency, the MSE value was significantly smaller than at the higher frequencies for all force application scenarios. For the body force, the highest MSE values were observed for the 3GHz signal in all regions except 4 and 6. For the press force, the highest MSE values were observed for the 4GHz signal in all regions except 1, 6 and 7.

Figures 6 and 7 show the plots of the reflection coefficient S_{11} vs the applied signal frequency obtained from the frequency sweep for both before and after a press force and body force were applied to all nine regions on the antenna surface. For all scenarios the resonant frequency of the antenna was observed at 1.1GHz. The resonant frequency was not seen to shift for any of the tested scenarios when the force was applied. However, small variations in the value of the reflection coefficient were observed at the resonant frequency. These changes are captured in Figure 8.

Figure 8 shows the change in the reflection coefficient S11 for each of the nine regions for the press force (a) and body force (b). For the press force, there was an increase in the reflected power for regions 2-4 and 7-9. The greatest increase in reflected power of 1.05dB was seen for region 4 and the smallest increase in power of 0.10dB for region 8. For regions 1, 5-6, there was a decrease in the reflected power. The greatest decrease of 0.13dB was observed for region 6 and the smallest decrease of 0.09dB was seen at region 5. For the application of the body force, all regions showed a decrease in the reflected power due to the bending of the antenna and underlying tissue. The greatest decrease of 0.84dB was observed for region 4. For region 1, there was little to no change in the reflected power with a decrease of 0.02dB being produced.

5. Analysis

Based on the information obtained for each of the force application scenarios the antenna structure was seen to have undergone significant flexing with various bending forms observed and displacement as much as 3.16mm produced. All of the observed deformations of the antenna structure and underlying tissue were not confined to a single plane but were complex multi-planar changes in shape. For the bending of the antenna structure, it was noted that the greatest displacement was achieved when the acting force (press or body force) was along the vertical or horizontal axis as compared to application at the diagonals. The observed trend in the deforming and displacement of the antenna structure and underlying tissue can be attributed to the fact that application of the press or body force to the ends of the antenna structure (regions 2, 4, 6 and 8) allow for the body of the antenna to act as a fulcrum and amplify the effect of the applied force.

Finally, action of the press and body force through the centre of the body of the antenna and underlying tissue (region 9) was seen to produce the smallest variations in displacement (0.20mm and 0.57mm, respectively). The significantly smaller changes in displacement may be due to the body of the antenna having resisted being bent and stretched through its centre.

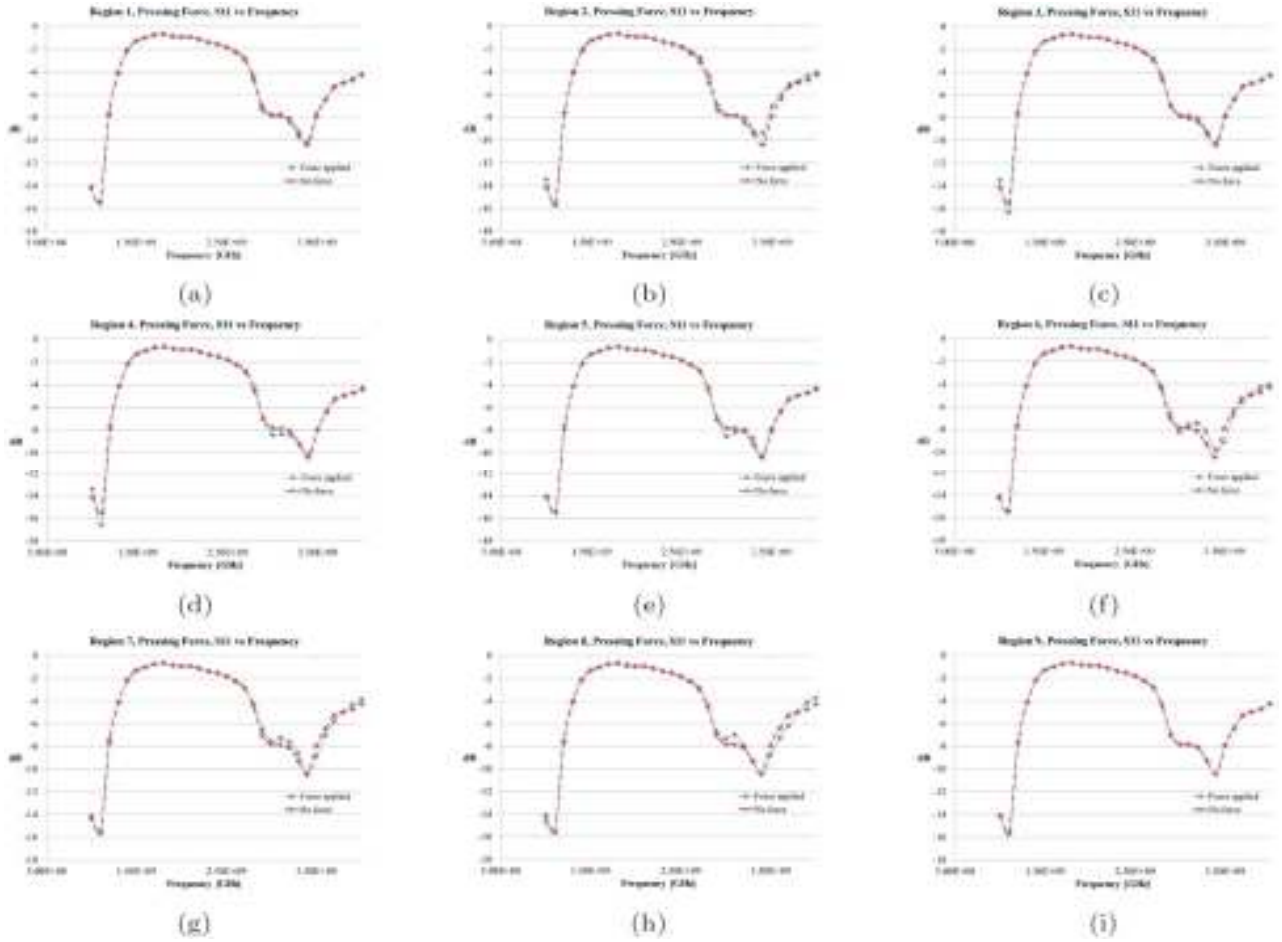

Figure 6. Plot of the reflection coefficient S11 vs frequency for before and after application to all nine regions of the action of pressing forces

It is worth noting that for all test scenarios the antenna structure was not seen to undergo destructive deformation (resulting in a rupture and/or tear) but was able to bend and conform to the movement of the underlying body tissue. This observed behaviour of the antenna structure lends support to the use of Nylon as a flexible substrate material for the antenna.

For the antenna performance, the antenna structure and body model prior to the application of a body or press force was seen to achieve resonance at 1.1GHz with a lesser resonant point at 3.4GHz. For all instances of force application (body and press force) it was noted that the resonant frequency points did not shift. Thus, the antenna resonant frequency showed good stability under deformation due to both press and body forces acting over its surface. This stability may be due to the fact that although the antenna structure underwent deformation due to the force, the deformation did not result in a significant change in the antenna geometry and/or dimensions.

While good stability was achieved for the antenna resonant frequency, variations were noted in the reflection coefficient S11. For the body force acting on all regions of the antenna there was a resultant reduction in the transmission power. The reduction in the transmission power can be considered as a result of the net movement and deforming of the antenna and the underlying tissue. In particular, the movement of the tissue layers and blood vessel would create a change in the resultant permittivity below the antenna surface and therefore would affect the antenna performance. Another key contributor to the reduction in the reflection coefficient S11 would be which section of the antenna's surface was shifted. It was noted that motion and deformation which most impacted the geometry of the antenna's conductive pattern and the microstrip line resulted in the greatest reduction in the transmission power.

For the press force testing, a reduction in the reflection coefficient S11 was observed for only three regions (region 1, 5 and 6). For all other regions of force application, an increased in S11 was observed. It was noted that the regions which produced the increase in the transmission power were regions where the applied force resulted in the microstrip line being pressed into the epidermis and dermis of the user.

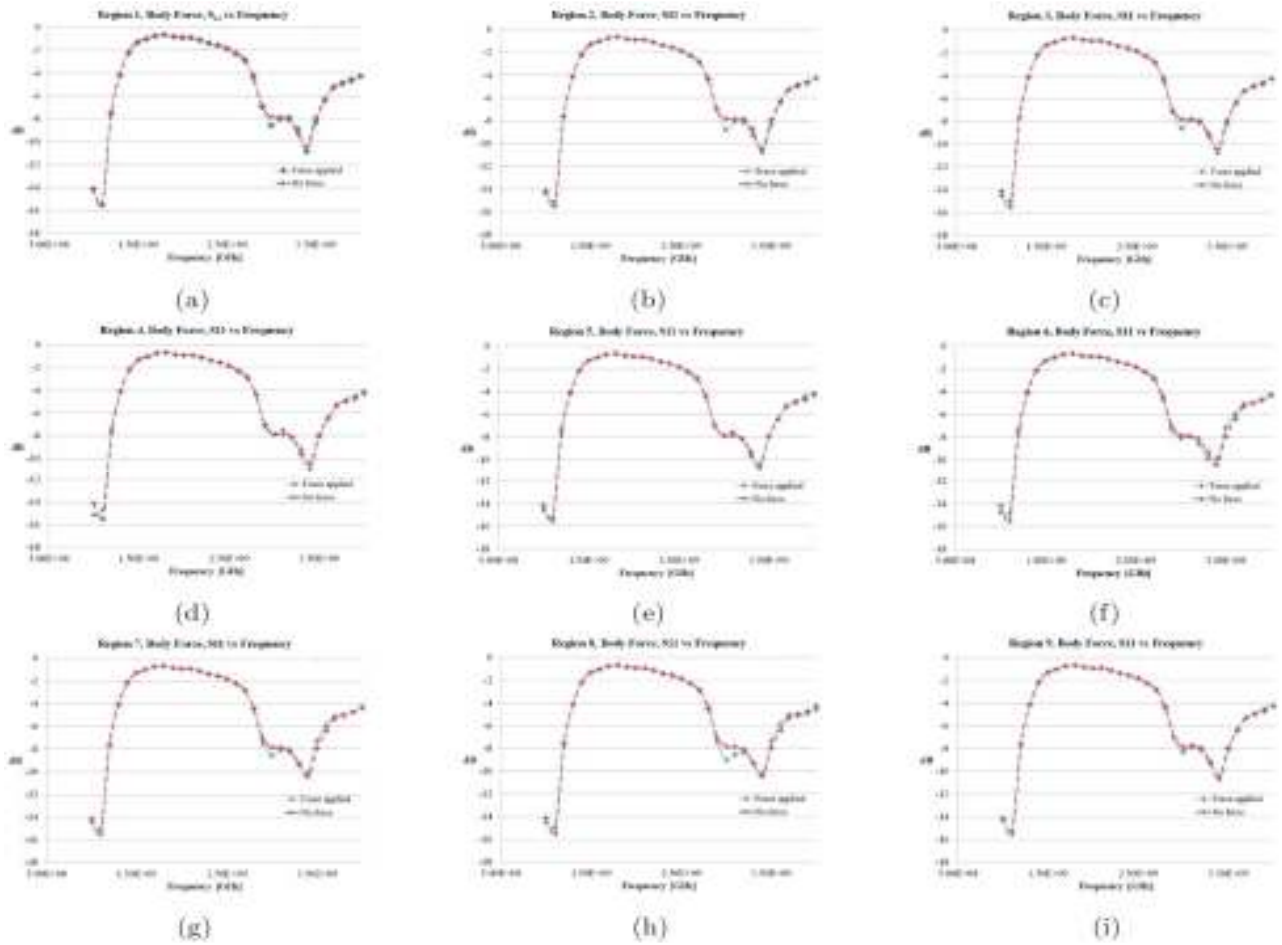

Figure 7. Plot of the reflection coefficient S11 vs frequency for before and after application to all nine regions of the action of body forces

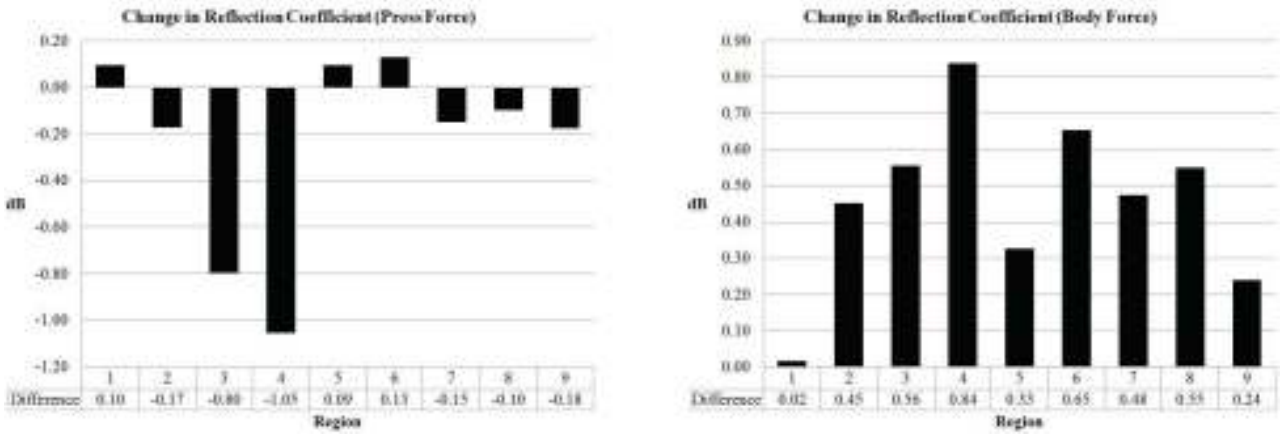

(a) (b)

Figure 8. Plots of the change in reflection coefficient vs region (a) pressing forces (b) body forces

This observation is particular significant since it illustrates that the underlying skin layers are contributing to an increase in the transmission power of the antenna. This behaviour can have possible consequences for the safe operation of such antenna structures.

The radiation pattern of the antenna was found to be largely unaffected at 1GHz due to the action of the press and body force. The radiation pattern at 1GHz was also found to be very symmetric in all planes and this symmetry was seen to be unaffected by the action of the applied forces (press and body force).

This characterisation shows that the antenna structure is resilient to the application of forces acting on it. The radiation patterns at the higher frequencies (3GHz, 4GHz), with no force applied to the antenna showed an increased in distortion and fell further afield for increased signal frequency. It was also observed that as the test frequency was increased the radiated signal was seen to become increasingly directional allowing the signal to penetrate further into the underlying tissue layers and surrounding air domain. The application of the force to the structure was seen to further increase the distortion of the radiated pattern. The signal was observed to fall even further afield, reaching deeper into the tissue layers and surrounding air domain. This result was of particular significance since the action of the force on the antenna and tissue layers resulted in the radiated signal penetrating further into the tissue as compared to when no force was acting.

The variation of the radiation pattern at the higher frequencies in response to the press and body forces can be attributed to the resultant displacement. The greatest displacement recorded was 3.16mm which would be equivalent to the wavelength of a frequency of approximate order of magnitude of GHz. As the applied signal frequency is increased and approaches multiples of the equivalent frequency (of the displacement) the distortion and spread of the radiation pattern would be more pronounced. The behaviour of the antenna structure at the higher frequencies can allow the structure to be adopted for sensing applications which require signal penetration further into the underlying tissue. However, the responsiveness of the antenna structure to deformations would require that some form of signal compensation is undertaken to allow for signal changes due to the deformation of the underlying tissue. The responsiveness of the antenna structure to the application of the force and the resultant deformation can allow the antenna to be used as a means to potentially monitor for press and body forces to the tissue.

The results from this work would suggest that the antenna structure as designed using the Nylon substrate would demonstrate good performance stability as regards the reflection coefficient S11, resonant frequency and general mechanical strength. The observed increased in transmission power for the scenarios involving the structure pressed into the flesh represents another area of interest for further investigation. The results obtained vis-a-vis the directionality and increased field penetration at higher frequencies presents possible opportunities for applying the antenna structure as a sensor targeting deeper tissue layers. Further investigation of the work would be conducted through more detailed simulation studies which are reinforced by building the antenna structure using the proposed materials and 3D printing processes and testing of the antenna structures in the identified frequency range of 700MHz-4GHz.

6. Conclusions

The simulation work conducted allowed for the examination of a PIFA antenna structure which was constructed using a Nylon substrate and which was subjected to various forces applied to nine different zones of the antenna surface. In addition, the antenna behaviour was considered in the context of it being present on the surface of a user's skin. The skin surface and underlying tissue were suitably represented both geometrically and with their assigned mechanical and electrical properties. The examination highlighted the extent of physical deformation possible when simple forces are applied to the antenna structure.

The stability of the antenna structure when subjected to forces was also demonstrated in terms of its reflection coefficient S11, resonant frequency and physical resilience. The work also revealed the interesting behaviour of the antenna when pressed into the body of the user, namely an increase in the reflection coefficient. The variation of the antenna radiation pattern both directionally as well as the increase in its far-field reach as the applied signal frequency was increased was noted. Also, of interest was the change in the radiation pattern at higher frequencies due to the deformation of the antenna and tissue when press and body forces were applied. This characterisation of the antenna behaviour at higher frequencies may present opportunities for the antenna structure to be adopted as a sensor.

Further work is proposed to examine the impact of the antenna structure on the underlying skin layers when varying levels of indentation into the skin are achieved. Work is also proposed to examine a more realistic representation of a 3D printed substrate (which considers for e.g. the existence of print-line boundaries and surface undulations). This work will be conducted through the creation of more detailed simulation models and the creation of prototype antenna structures.

References:

Andreuccetti, D., Fossi, R., and Petrucci, C. (1997), "An internet resource for the calculation of the dielectric properties of body tissues in the frequency range 10 Hz-100 GHz*",* Retrieved from http://niremf.ifac.cnr.it/tissprop

Bai, Q., and Langley, R. (2009), "Wearable ebg antenna bending and crumpling", *Proceedings of the Antennas and Propagation Conference, 2009*, Loughborough, November 16, pp. 201-204.

Bai, Q., and Langley, R. (2012), "Crumpling of pifa textile antenna", *IEEE Transactions on Antennas and Propagation,* Vol.60, No.1, pp.63-70.

Bai, Q., Rigelsford, J., and Langley, R. (2013), "Crumpling of microstrip antenna array", *IEEE Transactions on Antennas and Propagation*, Vol.61, No.9, pp.4567-4576.

Balanis, C.A. (1992), "Antenna theory: A review", *Proceedings of the IEEE*, Vol.80, No.1, pp.7-23.

Bandodkar, A.J., Jeerapan, I., and Wang, J. (2016), "Wearable chemical sensors: Present challenges and future prospects", *ACS Sensors*, Vol.1, No.5, pp.464-482.

Bevelacqua, P.J. (2016), *PIFA - The Planar Inverted-F Antenna*. Retrieved from http://www.antenna-theory.com/antennas/patches/pifa.php

Cameron, J.R., Skofronick, J.G., Grant, R.M., and Siegel, E. (1993), "Medical physics: Physics of the body", *American Journal of Physics*, Vol.61, No.12, pp.1156-1156.

Case, M.A., Burwick, H.A., Volpp, K.G., and Patel, M.S. (2015), "Accuracy of smartphone applications and wearable devices for tracking physical activity data", *Journal of the American Medical Association*, Vol.313, No.6, pp.625-626.

Casula, G.A., Michel, A., Montisci, G., Nepa, P., and Valente, G. (2017), "Energy-based considerations for ungrounded wearable uhf antenna design", *IEEE Sensors Journal*, Vol.17, No.3, pp.687-694.

Elias, N., Samsuri, N., Rahim, M., and Othman, N. (2013), "Investigation of crumpling effects on em absorption and antenna performance at 2.4 ghz", *Proceedings of the RF and Microwave Conference, 2013*, (IEEE International), Penang, December 9, pp. 395-399.

Hall, P.S., and Hao, Y. (2006), "Antennas and propagation for body centric communications", *Proceedings of the first European Conference on Antennas and Propagation, 2006.* Nice, November 6, pp.1-7.

Hertleer, C., Tronquo, A., Rogier, H., Vallozzi, L., and van Langenhove, L. (2007), "Aperture-coupled patch antenna for integration into wearable textile systems", *IEEE Antennas and Wireless Propagation Letters*, Vol.6 , pp.392-395.

Liang, X., and Boppart, S.A. (2010), "Biomechanical properties of in vivo human skin from dynamic optical coherence elastography", *IEEE Transactions on Biomedical Engineering,* Vol.57, No.4, pp.953-959.

Matthews, J., and Pettitt, G. (2009), "Development of flexible, wearable antennas", *Proceedings of the 3rd European Conference on Antennas and Propagation,* Berlin, March 23, pp. 273-277.

Mertz, L. (2016), "Are wearables safe?: We carry our smart devices with us everywhere-even to bed-but have we been sleeping with the enemy, or are cautionary tales overinflated?" *IEEE Pulse*, Vol.7, No.1, pp.39-43.

Murai, M., Lau, H.-K., Pereira, B.P., and Pho, R.W. (1997), "A cadaver study on volume and surface area of the fingertip", *The Journal of Hand Surgery*, Vol.22, No.5, pp.935-941.

Pantelopoulos, A., and Bourbakis, N.G. (2010), "A survey on wearable sensor-based systems for health monitoring and prognosis", *IEEE Transactions on Systems, Man, and Cybernetics, Part C (Applications and Reviews)*, Vol.40, No.1, pp.1-12.

Peebles, L., and Norris, B. (2003), "Filling gaps in strength data for design", *Applied Ergonomics*, Vol.34, No.1, pp.73-88.

Rais, N., Soh, P.J., Malek, F., Ahmad, S., Hashim, N., and Hall, P. (2009), "A review of wearable antenna", *Proceedings of the Antennas and Propagation Conference*, Loughborough, November 16, pp.225-228.

Rogier, H. (2015), "Textile antenna systems: design, fabrication, and characterisation", In: Tao, X. (ed), *Handbook of Smart Textiles*, Springer, Switzerland, pp.433-458.

Salonen, P., Sydanheimo, L., Keskilammi, M., and Kivikoski, M. (1999), "A small planar inverted-f antenna for wearable applications", *Digest of Papers (Proceedings of) the third international symposium on Wearable Computers,* San Francisco, Oct ober18, pp.95-100.

Shakhirul, M., Jusoh, M., Sahadah, A., Nor, C., and Rahim, H.A. (2014), "Embroidered wearable textile antenna on bending and wet performances for uwb reception", *Microwave and Optical Technology Letters*, Vol.56, No.9, pp.2158-2163.

Shima, K., Tamura, Y., Tsuji, T., Kandori, A., Yokoe, M., and Sakoda, S. (2009), "Estimation of human finger tapping forces based on a finger pad-stiffness model", *Proceedings of the Annual International Conference of the IEEE on Engineering in Medicine and Biology Society*, Minneapolis, September 3, pp.2663-2667.

Soh, P.J., Vandenbosch, G.A., Ooi, S.L., and Rais, N.H.M. (2012), "Design of a broadband all-textile slotted pifa", *IEEE Transactions on Antennas and Propagation*, Vol.60, No.1, pp.379-384.

Sundarsingh, E.F., Velan, S., Kanagasabai, M., Sarma, A.K., Raviteja, C., and Alsath, M.G.N. (2014), "Polygon-shaped slotted dual-band antenna for wearable applications", *IEEE Antennas and Wireless Propagation Letters*, Vol.13, pp.611-614.

Authors' Biographical Notes:

Jeevan Persad *received his B.Sc. degree in Electrical and Computer Engineering at The University of the West Indies in 2003 and his Masters in Electronic Product Development from The University of Bolton in 2012. His areas of interest include the application of 3D printing to the manufacture of electronic assemblies.*

Sean Rocke *received his BSc in Electrical and Computer Engineering from The University of the West Indies in 2002, his Masters in Communications Management and Operational Communications from Coventry University in 2004, and his Ph.D. in Electrical and Computer Engineering from Worcester Polytechnic Institute in 2013. His areas of interest include signal processing and optimisation techniques relating to wireless communications management application and biosensor development and biological data mining, as well as and emergency communication systems.*

■